A MNG-TL Loop Antenna Array With Horizontally Polarized Omnidirectional Patterns

Kunpeng Wei, Zhijun Zhang, *Senior Member, IEEE*, Zhenghe Feng, *Fellow, IEEE*, and Magdy F. Iskander, *Life Fellow, IEEE*

***Abstract*—A horizontally polarized omnidirectional planar loop antenna that employs an artificial mu-negative transmission line (MNG-TL) is proposed. The MNG-TL is designed using periodically loaded parallel-plate lines. The reactive loading is inspired by the zeroth-order resonator (ZOR), which has a propagation constant of zero. Due to the unique property of an infinite wavelength, the MNG-TL loop antenna presented in this paper allows current along the loop to remain in phase so that a horizontal polarized omnidirectional pattern is generated. A series-fed array, which is composed of four MNG-TL loop antennas and operates at 2.4 GHz band, is designed, fabrication, and measured. The MNG-TL loop antenna array offers a horizontally polarized omnidirectional radiation pattern with enhanced gain of 6.5 $\sim$ 7.9 dBi and measured radiation efficiency exceeding 85% for covering bands. The concept extends the degrees of design freedom for horizontally polarized omnidirectional antenna array.**

***Index Terms*—Horizontal polarization, mu-negative transmission line (MNG-TL), omnidirectional loop antennas, zeroth-order resonator (ZOR).**

I. Introduction

During the last several years, polarization diversity has been considered as an optimized Multiple-input-multiple-output (MIMO) technique for rich multi-path communication environment [1]. In base stations, $\pm 45^{\circ}$ dual-polarized sector directional antennas are adopted to enhance the channel capacity and improve the system performances [2], [3]. However, in some applications, such as the wireless local area network (WLAN) systems or distributed MIMO systems [4], omnidirectional antennas are more appropriate due to their limited service areas involved. In the indoor or urban areas, although many current wireless systems are vertically polarized, the polarization of the propagating electromagnetic wave may change significantly after complicated multiple reflections or scatterings [5]. Hence, a horizontally polarized antenna with an omnidirectional pattern is preferred to harvest the polarization resource and maximize a system's capacity [6], [7]. Therefore, the design of a horizontally polarized omnidirectional antenna with an acceptable input impedance matching is desirable.

The small loop antenna with a uniform current distribution can act as a magnetic dipole to achieve the horizontally polarized radiation pattern. However, due to very small radiation resistance and high reactance, a small loop antenna is difficult to use due to challenges with impedance matching [8]. Although a larger loop antenna has a reasonable radiation resistance, the antenna currents distribution along the loop becomes non-uniform and hence could not yield a desired horizontally polarized omnidirectional pattern [9], [10]. Alford loop antenna in the wire type was first reported to achieve an omnidirectional horizontally polarization in [11]. Several kinds of modified Alford-loop-structure antennas [12]–[15] have been studied and introduced as a useful design for generating magnetic dipole radiation patterns. These designs, however, have some problems with input impedance matching and the uniformity of the currents along the loop. Recently, studies of left-handed (LH) metamaterials, which is based on periodic structures, have progressed rapidly. From a practical application standpoint, the transmission line approach of LH metamaterials has led to the realization of composite right/left-handed transmission line (CRLH-TL) [16]–[18]. The CRLH-TL has many unique properties such as supporting a fundamental backward wave (opposite group and phase velocities) and zero propagation constant ($\beta = 0$) with non-zero group velocity at the zeroth-order resonance [19]. A zeroth-order resonator omnidirectional antenna based on left-handed CL loading has been shown in [20]. The radiation efficiency, however, is low and the gain is about 0.3 dBi.

Recently, some segmented loop antennas have been reported for generate strong and even magnetic filed. Dobkin *et al.* firstly presented the segmented magnetic antenna consisting of a number of segments and each segment is composed of a metal line and a series lumped capacitor [21]. In this structure, segmenting and combining the parasitic inductance of each section with a lumped capacitor caused the large loop to behave similar to an electrically small antenna. It keeps the current in the same direction and provides a strong magnetic field. However this antenna is not an effective far field radiator, as the antenna is loaded by a discrete resistor to achieve good matching. Based on the method, several segmented antennas [22]–[25] have been presented for UHF near-filed RFID reader applications. However, the far field radiations are not taken into account in these antennas. Only magnetic field distribution and reading rate were paid close attention to. The current flowing along the segmented loop antennas, however, was

Manuscript received February 06, 2011; revised October 11, 2011; accepted October 17, 2011. Date of publication April 30, 2012; date of current version May 29, 2012. This work was supported in part by the National Basic Research Program of China under Contract 2009CB320205, by the National High Technology Research and Development Program of China (863 Program) under Contract 2007AA01Z284, and in part by the National Science and Technology Major Project of the Ministry of Science and Technology of China 2010ZX03007-001-01.

K. Wei, Z. Zhang, and Z. Feng are with State Key Lab of Microwave and Communications, Tsinghua National Laboratory for Information Science and Technology, Tsinghua University, Beijing 100084, China (e-mail: zjzh@tsinghua.edu.cn).

M. F. Iskander is with HCAC, University of Hawaii at Manoa, Honolulu, HI 96822 USA (e-mail: iskander@spectra.eng.hawaii.edu).

Color versions of one or more of the figures in this paper are available online at http://ieeexplore.ieee.org.

Digital Object Identifier 10.1109/TAP.2012.2194643

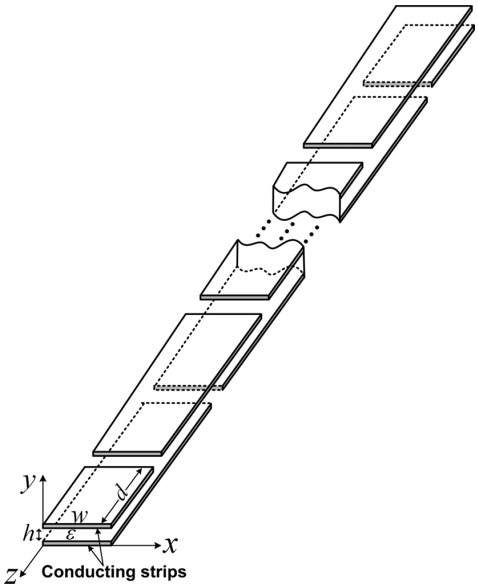

Fig. 1. Overall configuration of the proposed periodically loaded parallel-plate lines.

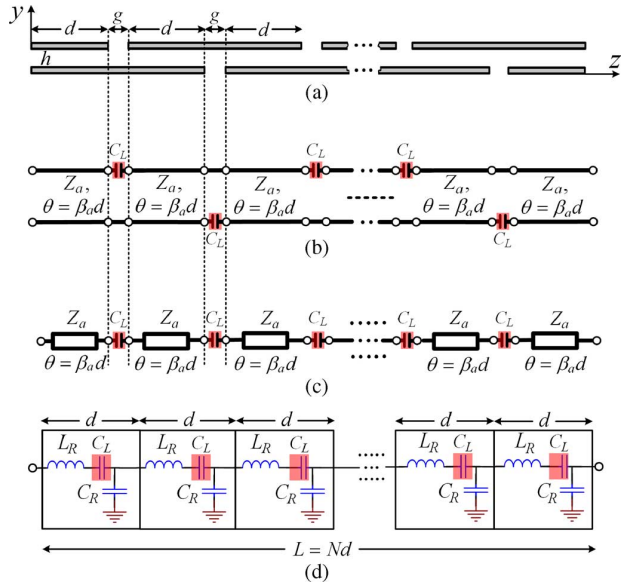

Fig. 2. (a) Side view of the proposed periodically loaded parallel-plate lines. (b) Corresponding equivalent circuit model neglecting the radiation resistances. (c) Corresponding equivalent TL circuit model. (d) Corresponding equivalent Lumped-element circuit model.

not absolutely in phase and uniform, so that the design was not suitable for horizontal polarized omnidirectional antennas. Furthermore, these existing papers about segmented antennas [21]–[25] don't have an appropriate theoretical explanation about the same directional currents of the large loop design.

In order to get a horizontally polarized omnidirectional pattern, the requirements of the phase and amplitude of the current along the loop are very strict. In this paper, a MNG-TL loop antenna with horizontally polarized omnidirectional pattern is realized by using periodically loaded parallel-plate lines. The approach is inspired by the segmented loop antennas for UHF near-field RFID applications [21]–[25]. The MNG-TL loop antenna proposed in this paper allows current along the loop to remain in phase and, hence, achieve a horizontally polarized omnidirectional pattern in the far-field. The investigation and theoretical explanation about the in-phase and uniform current distributions are being presented for the first time in this paper through the principle of the MNG-TL. To the authors' knowledge, it is the first time that the MNG-TL loop is applied for horizontally polarized omnidirectional antenna.

II. Principle of the Artificial MNG-TL Based on Periodically Loaded Parallel-Plate Lines

A. Periodically Loaded Parallel-Plate Lines

Fig. 1 shows the overall configuration of the proposed periodically loaded parallel-plate lines. The parallel-plate line in this structure consists of two parallel conducting strips of width w separated by a dielectric material of permittivity ε and height h. As shown in Fig. 2(a), the proposed structure is composed of a plurality of the parallel-plate transmission line sections periodically gap loaded with a period of d. All the parallel-plate transmission line sections have the same characteristic impedance Z_a and phase constant β_a. To determine the dispersion relation and resonances of the periodically loaded parallel-plate lines, the radiation resistances are neglected without affecting the resonance characteristic. Therefore, the corresponding equivalent circuit model is shown in Fig. 2(b), where the periodically loading series capacitance represents the coupling of the adjacent parallel-plate transmission line sections. The value of the capacitance can be estimated from a full-wave parameter extracting technique. This model can be further illustrated as a TL circuit model shown in Fig. 2(c), which is represented by a plurality of TL sections with series capacitances. In order to examine the resonances of the structure further, it is instructive to replace the TL sections with their equivalent distributed inductance L_R and capacitance C_R as shown in Fig. 2(d). It is clear that the proposed periodically loaded parallel-plate line is an artificial mu-negative transmission line (MNG-TL) structure. The MNG-TL supports an infinite wavelength at the zeroth-order resonance $(\beta = 0, \omega \neq 0)$, where the effective permeability is zero.

B. Resonance Characteristics

Suppose the transmission line section in Fig. 2(a) is a pure TEM line, the TEM mode solution can be obtained by solving Laplace's equation [26]. The characteristic impedance of the line will be:

$$Z_a = \frac{\eta h}{w} = 377\frac{h}{w\sqrt{\varepsilon_r}}. \tag{1}$$

The distributed inductance and capacitance per unit length can be found as:

$$\begin{cases} L'_R = \mu\frac{h}{w} \\ C'_R = \varepsilon\frac{w}{h} \end{cases}. \tag{2}$$

When the proposed periodically loaded parallel-plate line is open-ended or short-ended, it produces standing waves due the open/short boundary conditions and becomes a resonator with a length $L = Nd$, where N is the number of these sections. It is well-know that an infinite number of resonant modes exist in such resonator, satisfying

$$\beta_a L = \beta_a(Nd) = m\pi \quad (m = 0, 1, 2, \ldots) \tag{3}$$

where m is the resonance mode number of the resonator. The resonance frequencies are obtained by sampling the dispersion curve $\omega = \omega(\beta_a)$. By applying periodic boundary conditions (PBCs) related to the Bloch-Floquet theorem to the Lumped-element unit cell in Fig. 2(d), the dispersion relation will be as follows [18]

$$\cos\beta_a d = 1 - \frac{1}{2}\left(\frac{\omega^2 - \omega_{MZR}^2}{\frac{1}{L_R C_R}}\right) \tag{4}$$

where

$$\omega_{MZR} = \frac{1}{\sqrt{L_R C_L}}. \tag{5}$$

Here, $L_R(=L'_R d), C_R(=C'_R d)$ are in terms of the real LC lumped component (in F and H), respectively. To address the boundary conditions of periodically loaded parallel-plate line resonator, input impedances of open-ended and short-ended cases are separately calculated by (6), (7) [18]

In the *open-ended* case,

$$\begin{aligned} Z_{in}^{open} &= -jZ_c\cot(\beta_a L) \overset{\beta_a\to 0}{\approx} -jZ_c\frac{1}{\beta_a L} \\ &= -j\sqrt{\frac{Z'}{Y'}}\left(\frac{1}{-j\sqrt{Z'Y'}}\right)\frac{1}{L} = \frac{1}{NY}. \end{aligned} \tag{6}$$

In the *short-ended* case,

$$\begin{aligned} Z_{in}^{short} &= jZ_c\tan(\beta_a L) \overset{\beta_a\to 0}{\approx} jZ_c\beta_a L \\ &= j\sqrt{\frac{Z'}{Y'}}(j\sqrt{Z'Y'})L = NZ. \end{aligned} \tag{7}$$

By applying the conditions to the equivalent circuit of LC-based MNG-TL, input impedances can be rewritten as

$$\begin{cases} Z_{in}^{open} = \frac{1}{j\omega N C_R} \\ Z_{in}^{short} = \frac{N}{j\omega C_L} + j\omega N L_R \end{cases}. \tag{8}$$

Therefore, to obtain the ZOR resonance, the short-ended boundary condition must be applied to the MNG-TL resonators. The mu-zero resonant frequency f_{MZR} given in (5) is independent of the length of the resonator but depends only on the reactive loadings.

Without the periodically gap loaded arrangement, the structure is merely a uniform TEM transmission line, which exhibits a linear dispersion curve, starting from the origin ($\beta = 0$) of the dispersion diagram, as shown in Fig. 3(a). The periodic gap loading transforms the structure and it becomes a periodically reactive loaded transmission line, terminated by a short and with the modified dispersion curves and resonances shown in Fig. 3(b). In contrast to the unloaded parallel-plate transmission line, the proposed structure has the unique property of an infinite wavelength wave. In the case where $m = 0$, zeroth-order resonator can be excited and there is no phase shift across the resonator since phase shift is determined by $\varphi = -\beta d = 0$.

To verify the equivalent Lumped-element circuit model in Fig. 2(d), an eight-stage periodically loaded parallel-plate line short-ended resonator was full-wave simulated using Ansoft simulation software high frequency structure simulator (HFSS). The parameter values are chosen to be $d = 6$ mm, $g = 1.2$ mm, $h = 0.7$ mm and $w = 4$ mm respectively. It is designed on a low-cost teflon substrate with a dielectric constant $\varepsilon_r = 2.65$.

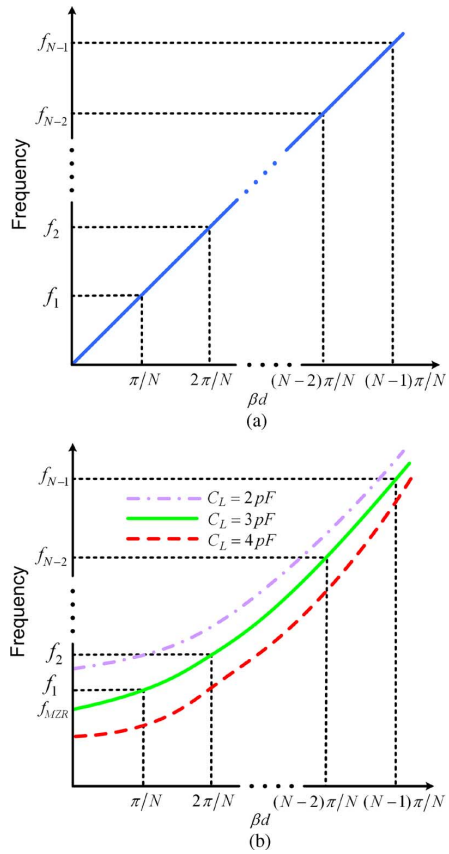

Fig. 3. Dispersion curves and short-ended resonances of (a) a unloaded parallel-plate transmission line and (b) a periodically loaded parallel-plate line computed by (4).

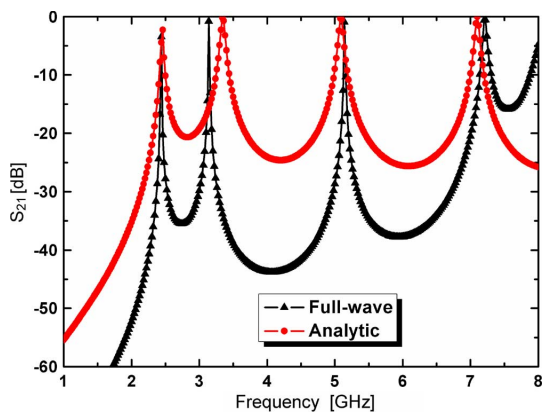

Fig. 4. Resonance modes of the eight-stage periodically loaded parallel-plate line short-ended resonator. The full-wave results correspond to the exact periodically loaded parallel-plate lines in Fig. 2(a).

The corresponding results are compared with theoretical analytic results of equivalent Lumped-element circuit model in Fig. 2(d). According to (1) and (2), the corresponding parameter can be found to be $Z_a = 40.7\ \Omega$, $L_R = 1.50$ nH and $C_R = 0.90$ pF. The periodically loading series capacitance $C_L = 2.5$ pF, which is obtained form a full-wave parameter extracting technique.

Fig. 4 shows that the analytical results of equivalent lumped-element circuit model follow the full-wave simulation very well.

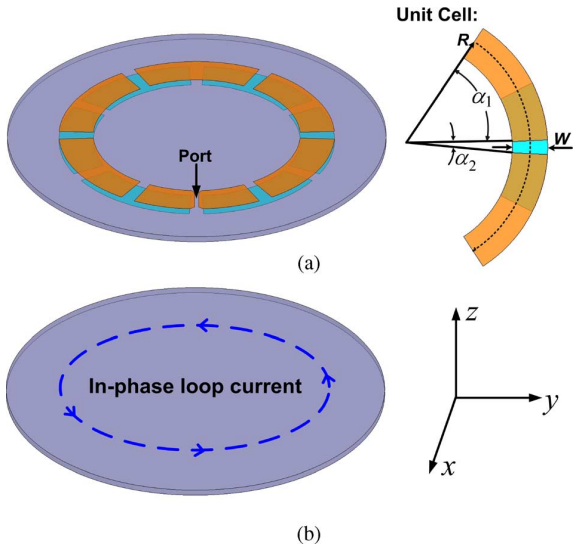

Fig. 5. (a) Geometry of the proposed MNG-TL loop antenna. (b) Equivalent in-phase loop current.

This confirms the proposed equivalent circuit model and validates its accuracy. Due to the infinite number of resonant modes existing, only the first four order resonance modes are compared. The slight differences in the results may be due to the fringing effects of the transmission line. It is, however, clear that the eight-stage periodically loaded parallel-plate line short-ended resonator has a zeroth order resonance mode ($f_{MZR} = 2.44$ GHz), which supports a unique property of an infinite wavelength. This property allows the current along the resonator to remain in phase.

III. Horizontally Polarized MNG-TL Loop With Omnidirectional Patterns

In this section, a horizontally polarized MNG-TL loop antenna with omnidirectional patterns is realized on the basis of the MNG-TL structure. The unit-cell for the proposed MNG-TL loop antenna is designed according to periodically loaded parallel-plate line. The input impedances as a function of the parameter values are examined. The width of the parallel-plate line, the thickness of the dielectric substrate and the number of the unit-cell are all factors that control the dispersion curve of the unit-cell and in effect the resonant frequencies. With the unique property of an infinite wavelength wave, the MNG-TL loop antenna allows current along the loop to remain in phase so that a horizontal polarized omnidirectional pattern is generated. To demonstrate this effect, simulation results and experimental verification of the proposed MNG-TL loop antenna with the MNG-TL loading are presented and discussed.

A. Realization of a Horizontally Polarized Omnidirectional Loop Antenna

The general model of the proposed MNG-TL loop antenna is shown in Fig. 5. In order to realize an in-phase loop current in Fig. 5(b), the loop antenna was constructed with periodic mu-negative transmission line (MNG-TL) metamaterial-based unit-cell. The unit-cell is based on the proposed periodically loaded parallel-plate lines discussed in Section II. The equivalent circuit for the unit-cell of Fig. 5(a) has been shown in Fig. 2(d). The left-handed series capacitance C_L was formed by the coupling of the adjacent parallel-plate transmission line sections. The unit-cell structure has the following parameters: a width W and radius R of the parallel-plate, the period angle α_1 and the gap angle of α_2. The periodic angle α_1 and the gap angle α_2 are related to the number of cells N by

$$\alpha_1 + \alpha_2 = \frac{360}{N}. \tag{9}$$

The proposed MNG-TL loop antenna is also designed on a low-cost teflon substrate with a dielectric constant $\varepsilon_r = 2.65$ and a thickness H.

Due to the left-handed series capacitance C_L, the effective permeability of the MNG-TL based unit-cell has negative, zero and positive values as mentioned in Section II. When the MNG-TL works at the mu-zero frequency f_{MZR}, it has a unique property that supporting a zero propagation constant ($\beta = 0$) with non-zero group velocity. At the zeroth-order resonance ($m = 0$), there is no phase shift across the resonator. So that the currents distribution along the loop remains in phase and could yield a desired horizontally polarized omnidirectional pattern. As shown in (5), by varying the series parallel coupled capacitance C_L or distributed inductance L_R of the MNG-TL unit cell, the mu-zero frequency f_{MZR} of the MNG-TL loop antenna can be controlled.

B. Antenna Design and Parametric Study

In the antenna design, the input impedance response can display important information about the designed antenna behavior, such as the impedance match, the resonant frequency and the bandwidth. Therefore, a parametric study focused on the input impedance of the MNG-TL loop antenna was considered. The input impedance ($Z_{in} = R + jX\Omega$) of the antenna implementation is computed using the finite-element method (FEM) based full-wave solver, Ansoft HFSS. A 50 Ω lump port is directly attached to the input edges of the loop and embedded to calculate the input impedance.

Theoretically, the resonance is independent of the total length and the unit-cell number. However, let us now include the radiation resistances of periodically loaded parallel-plate lines, R_r, the exact input impedance of (8) is modified as

$$Z_{in} = \frac{N}{j\omega C_L} + j\omega N L_R + N R_r. \tag{10}$$

It can be shown that the input impedance is also related to the unit-cell number. Therefore, the performances of the MNG-TL loop antenna with different unit-cell numbers are summarized in Table I. To exclude other alterable factors, the parameters of W, R, α_1 and α_2 have been changed correspondingly to keep the period and gap of each unit-cell same as in the prototype of Section II. As the number of unit-cells increases, the infinite wavelength frequency f_{MZR} approaches the value predicted by applying PBCs on a single unit-cell. It can be observed that the infinite wavelength frequency decreases slightly as the number of unit-cells increases. That is because in the particular case of MNG-TL loop antenna, boundary condition of the MNG

TABLE I
SUMMARY OF INPUT IMPEDANCE AND CORRESPONDING RESONANT FREQUENCY OF MNG-TL LOOP ANTENNA VERSUS UNIT-CELL NUMBER

Unit-cell number (N)	α_1	α_2	R (mm)	Resonant frequency (GHz)	Input impedance (Ω)
8	81°	9°	9.4	2.56	20.8-6.2j
12	54°	6°	14	2.44	50.7+0.6j
24	40.5°	4.5°	18	2.31	98.4-40j

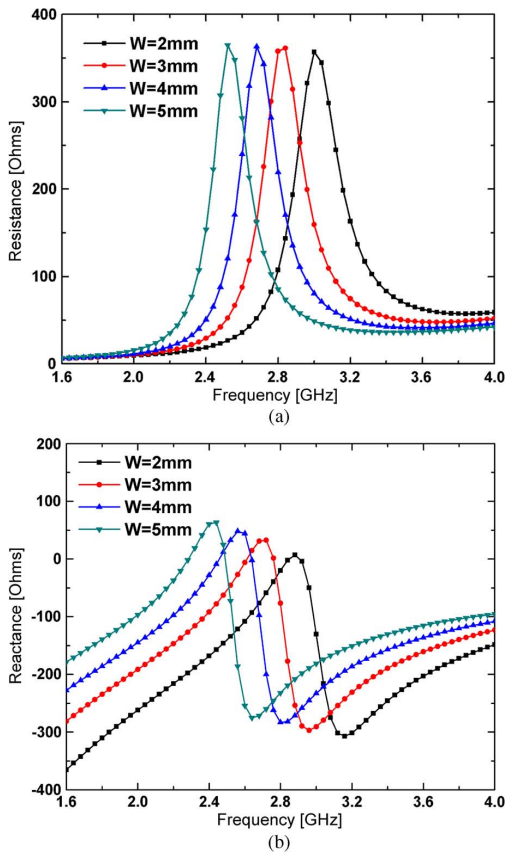

Fig. 6. Twelve-stage MNG-TL loop antenna input impedance for four different width ($H = 0.7$ mm). (a) Real part (R). (b) Imaginary part (X).

resonator could not be simply considered as the short-ended boundary. Furthermore, the impedance matching is also affected with the unit-cell number increasing.

The unit-cell number has been chosen to be 12 and other dimensions of the MNG-TL loop antenna are identical to those discussed in Table I, such as $\alpha_1 = 54°$, $\alpha_2 = 6°$ and $R = 14$ mm. To investigate the effect of the width W of the parallel-plate line, the input impedance of the twelve-stage MNG-TL loop antenna is calculated for four different widths: $W = 2$ mm, $W = 3$ mm, $W = 4$ mm and $W = 5$ mm. In general, a reactance value must be zero for good impedance matching. As shown in Fig. 6, the resonant frequency decreases as the width of the parallel-plate lines increases.

The behavior of the thickness H of twelve-stage MNG-TL loop antenna on the input impedance has been also studied. Here various thicknesses H of the dielectric substrate are chosen from 0.5 mm to 1.1 mm, and the width of the parallel-plate

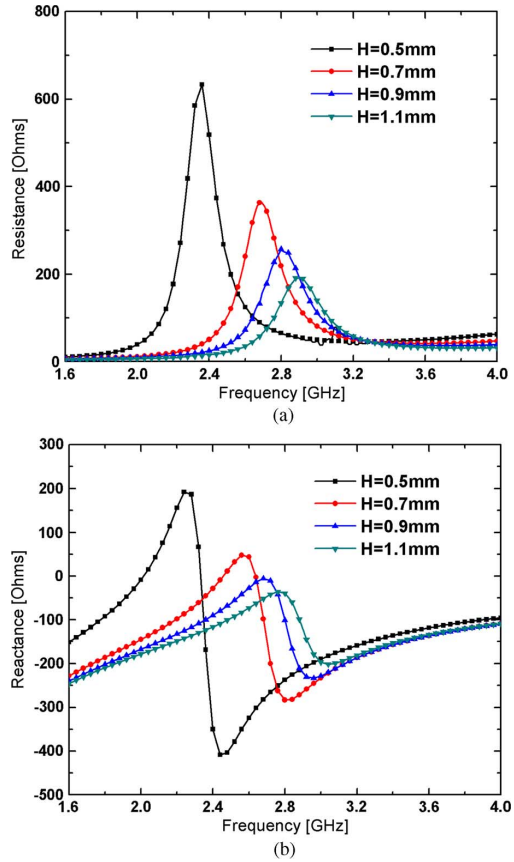

Fig. 7. Twelve-stage MNG-TL loop antenna input impedance for various thicknesses of the dielectric substrate ($W = 4$ mm). (a) Real part (R). (b) Imaginary part (X).

lines is fixed at $W = 4$ mm. The simulation results for various thicknesses of the dielectric substrate are shown in Fig. 7. It's shown that the input impedance for matching the antenna can be controlled by the substrate thickness H. As the substrate thickness H decrease, the peak of the impedance becomes larger and more keen-edged. This is due to the fact that the space between the parallel-plate lines determined by the substrate thickness H, which is related to the intensity of the coupling between the adjacent parallel-plate lines and characteristic impedance of parallel-plate transmission line sections. For instance, a good impedance matching is obtained at a thickness H of 0.7 mm and the resonant frequency of 2.44 GHz, as shown in Fig. 7. Consequently, an optimized impedance matching can be determined according to the width W of the parallel-plate lines and the thickness H of the dielectric substrate.

C. Simulation and Experiment Results of the Proposed MNG-TL Loop Antenna

A MNG-TL loop antenna was designed and simulated using Ansoft's HFSS full-wave simulator. The final design of the antenna has the following parameters: $R = 14$ mm, $W = 4$ mm, $H = 0.7$ mm, $N = 12$, $\alpha_1 = 54°$, $\alpha_2 = 6°$. Thus, the perimeter of the MNG-TL loop antenna is about 1.2 λ_0 at 2.4 GHz. To validate the design, a prototype of the proposed MNG-TL loop antenna has been fabricated and measured. Ferrite beads were used to cover the most part of test cable that is close to the loop antenna. The length of ferrite-bead

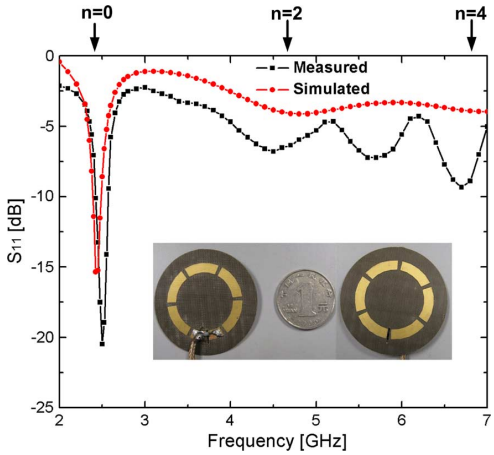

Fig. 8. Simulated and measured reflection coefficient values S_{11} of the proposed MNG-TL loop antenna.

covered section of the feed cable is about 50 mm. Fig. 8 shows the measured and simulated S_{11} of the constructed prototype. The measured data in general agrees with the simulated results. Several resonances are observed, which can be explained by conventional resonances given in (11). Derived from (3), this gives the relationship between the resonance number n, the total length L of the loop antenna, and the wavelength λ_a of the current along the loop

$$L = n\frac{\lambda_a}{2}. \tag{11}$$

A resonance in the $m = 0$ mode (ZOR) was observed at 2.44 GHz by measurement, where the wavelength is infinite and the phase constant is zero. It is shown that the fractional bandwidths of -10 dB reflection coefficient were simulated and measured as 110 MHz (2.38–2.49 GHz, 4.5%) and 140 MHz (2.42–2.56 GHz, 5.7%), respectively. These values are slightly different possibly due to the metallic loss and additional losses of the SMA connectors and cables during the prototype fabrication and measurement.

To investigate the radiation pattern of the MNG-TL loop antenna intuitively, the surface currents distribution for both the twelve-stage MNG-TL loop antenna and conventional right-handed 1.2 λ_0 loop antenna are shown in Fig. 9. Currents in the case of conventional 1.2 λ_0 loop antenna become non-uniform with the phase-shift and have the same direction at both the top and bottom edges along the loop, giving a maximum radiation in the broadside. However, the MNG-TL loop antenna works at the zeroth-order resonance with a zero propagation constant $(\beta = 0)$, so that no phase shift along the loop. As shown in Fig. 9(a), the proposed MNG-TL loop antenna allows a uniform in-phase current along the loop, which is identical to that of a small-loop antenna. Therefore, it can be considered close to a magnetic dipole to achieve a horizontally polarized omnidirectional radiation pattern. As discussed in Section III-B, a good impedance matching can be obtained by tuning the parameters of the MNG-TL loop without any additional matching network. To verify that the MNG-TL loop antenna has a horizontally polarized omnidirectional radiation pattern, the radiation characteristics of the proposed MNG-TL loop antenna were also studied. An ETS 3-D chamber was used to measure the pattern

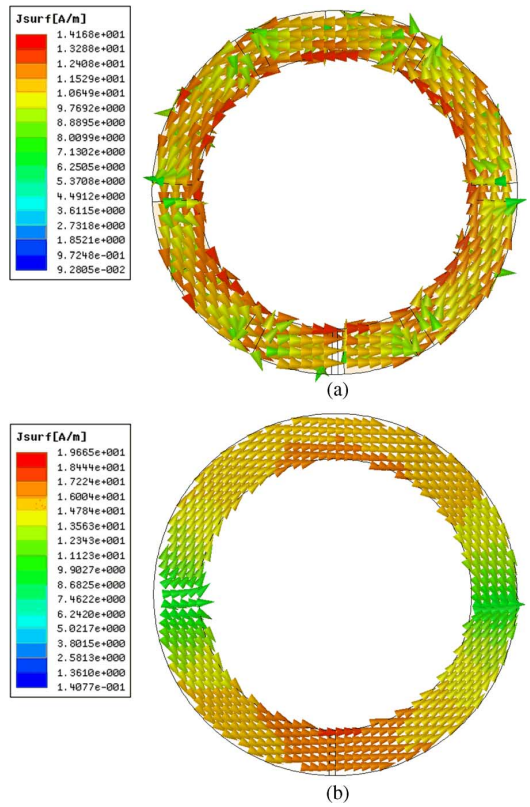

Fig. 9. Simulated surface currents distribution for (a) twelve-stage MNG-TL loop antenna and (b) conventional right-handed 1.2 λ_0 loop antenna.

of the MNG-TL loop antenna. Measured and simulated normalized E-planes and H-planes patterns for the proposed MNG-TL loop antenna at 2.44 GHz are presented in Fig. 10(a), (b), respectively. The measured maximum gain of the antenna was 2.3 dBi. From the results, the co-polarization and cross-polarization corresponds to the radiated electric field in the φ-direction and in the θ-direction. Moreover, good horizontally polarized omnidirectional radiation in the azimuth plane (x-y plane) with small gain variation less than 1.3 dB is obtained. Compared to the traditional Alford loop [14], [15], the proposed MNG-TL loop antenna is more compact. The area of the proposed MNG-TL loop antenna is two thirds of the volume of the traditional Alford loop [14], [15].

IV. Four-Element Series-Fed MNG-TL Loop Antenna Array

A horizontally polarized MNG-TL loop antenna with omnidirectional patterns has been realized in Section III. However, for many applications such as WLAN access point, the MNG-TL loop antenna gain of about 2.3 dBi is not sufficient. A series-fed array can be used to enhance the gain of the MNG-TL loop antenna. As shown in Fig. 11(a), the array is composed of four series-fed MNG-TL loop antenna elements with identical dimensions as discussed in Section III-C. The equivalent circuit of the feeding structure is shown in Fig. 11(b). To keep all radiating elements excited in-phase, the distance of the adjacent elements should be chosen to be a wavelength. A 25 ω parallel-plate line is applied to feed the designed loop array and a quarter wavelength impedance transformer is used to achieve

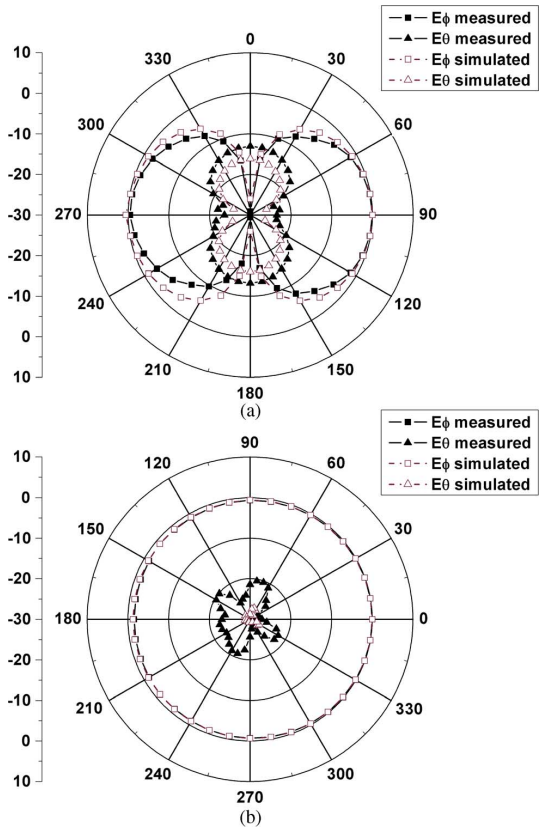

Fig. 10. Normalized measured and simulated radiation patterns for the proposed MNG-TL loop antenna at 2.44 GHz. (a) E-planes. (b) H-planes.

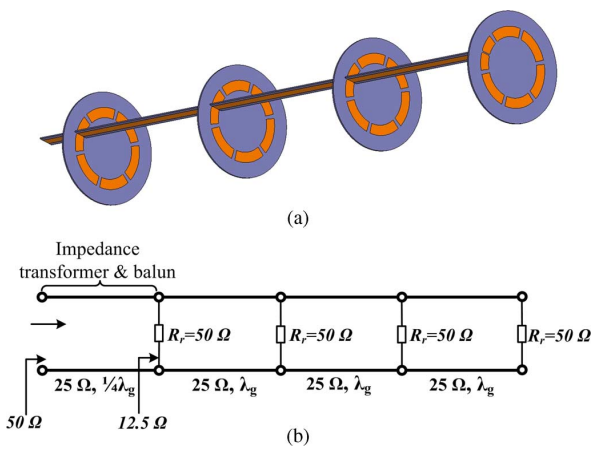

Fig. 11. Four-element series-fed MNT-TL loop antenna array. (a) Geometry of the prototype. (b) Equivalent circuit.

a good impedance matching. The quarter wavelength transmission line also functions as a balun, which converts the unbalanced feed of a SMA connector to a balanced parallel-plate line.

The proposed antenna array in Fig. 11(a) is fabricated and measured to verify the above discussed results. The photo of the fabricated prototype is shown in Fig. 12. Fig. 13 shows the simulated and measured reflection coefficient of the designed antenna array. Good agreement between the measurement and the simulation has been obtained. Note that a resonant mode is excited with good impedance matching at about 2.4 GHz and the VSWR 2:1 ($S11 < -10$ dB) impedance bandwidth is about 260 MHz (2320–2580 MHz), which covers WLAN band. The

Fig. 12. Photography of the fabricated prototype.

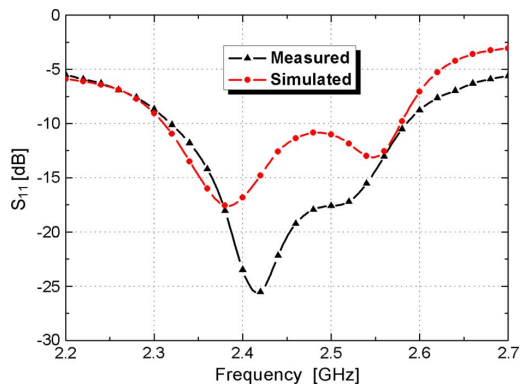

Fig. 13. Simulated and measured reflection coefficient values S_{11} of the proposed MNG-TL loop antenna array.

measured radiation patterns at 2.44 GHz of MNG-TL loop antenna array are presented in Fig. 14. Measurements at other operating frequencies across the 2.4 GHz band (not shown here for brevity) also show similar radiation patterns as plotted here, which indicates that the radiation patterns are stable in the desired operating band. From these results, it is clear that good omnidirectional radiation with horizontal polarization in the azimuth plane (x-y plane) with small gain variation is obtained. In the elevation planes (x-z and y-z planes), HBPW (half-power beamwidth) of the proposed loop array are 20° at 2.44 GHz, comparing to 74° HBPW for MNG-TL loop element discussed in Section III-C.

Fig. 15 shows the measured peak antenna gain and efficiency as a function of the operating frequency. The measured enhanced gain of the antenna array with the case varied from 6.5 to 7.9 dBi. The ETS 3-D chamber can also provide an estimated value of the radiation efficiency of the measured antenna. The efficiency is defined as the ratio of radiated power versus total available power from power source. Thus the efficiency value includes all impacts from mismatch loss, dielectric loss, conductor loss and matching component loss. The efficiency of the designed MNG-TL loop antenna array was found to exceed 85% in the covering bands. Measured gain variation of the designed array is shown in Fig. 16. The gain variation in the azimuth plane is below 2.1 dB over the WLAN band, which represents a stable omnidirectional coverage.

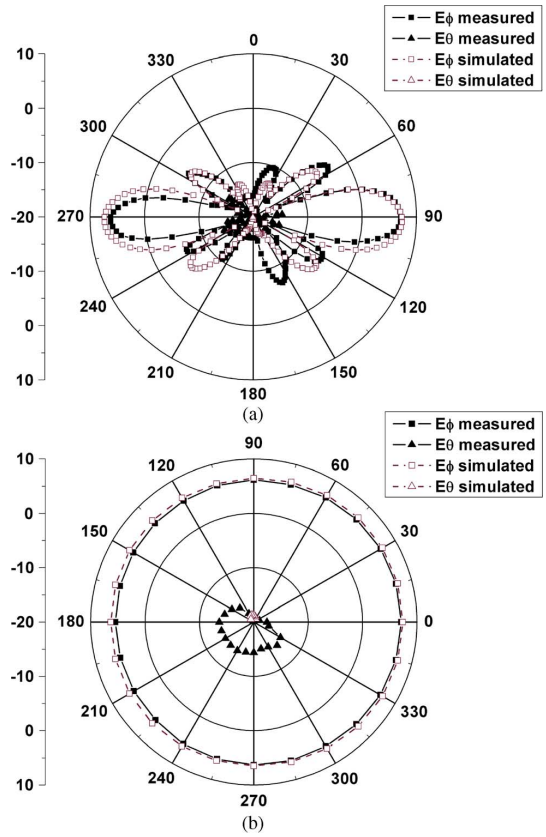

Fig. 14. Measured and simulated radiation patterns for the proposed MNG-TL loop antenna array at 2.44 GHz. (a) E-planes. (b) H-planes.

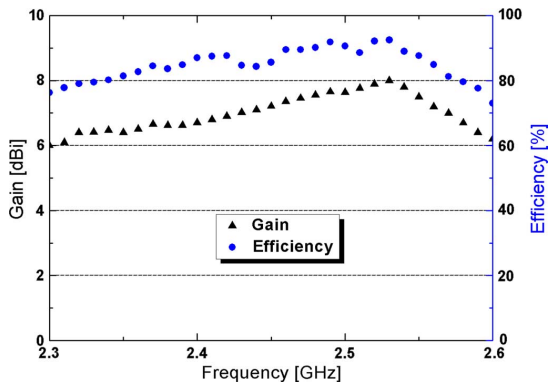

Fig. 15. Measured antenna gain and efficiency of the proposed MNG-TL loop array.

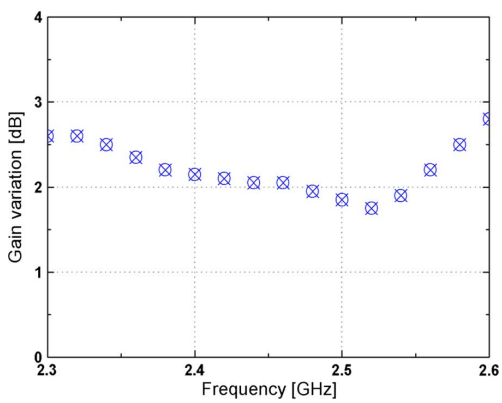

Fig. 16. Measured gain variation in the azimuth plane versus the operating frequency.

V. Conclusion

In this paper, a horizontally polarized omnidirectional loop antenna is proposed, designed and experimentally tested. The proposed loop antenna is based on a periodic design approach and the unit-cell is an artificial mu-negative transmission line (MNG-TL) realized by periodically loaded parallel-plate lines. With the MNG-TL reactive loading, the proposed loop antenna supports an infinite wavelength at the zeroth-order resonance $(\beta = 0, \omega \neq 0)$. At the zeroth-order resonance, there is no phase shift across the loop. So that the currents distribution along the loop remains in phase and could yield a desired horizontally polarized omnidirectional pattern. A parametric study focused on the input impedance of the MNG-TL loop antenna is presented to achieve good impedance matching. Furthermore, to meet the gain requirements of some applications such as WLAN access point, a four-element series-fed array is proposed. The four-element MNG-TL loop antenna array offers horizontally polarized omnidirectional radiation patterns with enhanced gain of 6.5 $\sim$ 7.9 dBi. The proposed horizontally polarized omnidirectional MNG-TL loop antenna also has the performance that is suitable to be a companion of a vertical polarized antenna array for polarization diversity and other practical applications.

References

[1] R. G. Vaughan, "Polarization diversity in mobile communications," *IEEE Trans. Veh. Technol.*, vol. 39, no. 3, pp. 177–186, Aug. 1990.

[2] J. Liu, Y. Yuan, L. Xu, R. Wu, Y. Dai, Y. Li, L. Zhang, M. Shi, and Y. Du, "Research on smart antenna technology for terminals for the TD-SCDMA system," *IEEE Commun. Mag.*, pp. 116–119, Jun. 2003.

[3] M. Barba, "A high-isolation, wideband and dual-linear polarization patch antenna," *IEEE Trans. Antennas Propag.*, vol. 56, no. 5, pp. 1472–1476, May 2008.

[4] R. Ibernon-Fernandz, J. Molina-Garcia-Pardo, and L. Juan-Llacer, "Comparison between measurements and simulations of conventional and distributed MIMO system," *IEEE Antennas Wireless Propag. Lett.*, vol. 7, pp. 546–549, 2008.

[5] D. Chizhik, J. Ling, and R. A. Valenzuela, "The effect of electric field polarization on indoor propagation," in *Proc. IEEE Int. Conf. Universal Personal Communications*, Oct. 1998, vol. 1, pp. 459–462.

[6] I. Pele, Y. Mahe, A. Chousseadud, S. Toutain, and P. Y. Garel, "Antenna design with control of radiation pattern and frequency bandwidth," in *Proc.IEEE Antennas Propag. Soc. Int. Symp.*, 2004, vol. 1, pp. 783–786.

[7] D. S. Kim, C. H. Ahn, Y. T. Im, S. J. Lee, K. C. Lee, and W. S. Park, "A windmill-shaped loop antenna for polarization diversity," in *Proc. IEEE Antennas Propag.-Soc. Int. Symp.*, Honolulu, HI, Jun. 2007, pp. 361–364.

[8] C. A. Balanis, *Antenna Theory: Analysis and Design*, 3rd ed. Hoboken, NJ: Wiley-Interscience, 2005.

[9] S. V. Shynu and M. J. Ammann, "A printed CPW-fed slot-loop antenna with narrowband omnidirectional features," *IET Microw. Antennas Propag.*, vol. 3, no. 4, pp. 673–680, 2009.

[10] T. A. Dnidni, H. Lee, Y. Lim, and Q. Rao, "Wideband high efficiency printed loop antenna design for wireless communication systems," *IEEE Trans. Antennas Propag.*, vol. AP-54, pp. 873–878, 2005.

[11] A. Alford and A. G. Kandoian, "Ultra-high frequency loop antenna," *Trans. AIEE*, vol. 59, pp. 843–848, 1940.

[12] H. R. Chuang, "Omni-Directional Horizontally Polarized Alford Loop Strip Antenna," U.S. Patent 5,767,809, Jun. 16, 1998.

[13] C. C. Lin and H. R. Chuang, "A 2.4 GHz planar printed antenna with omni-directional horizontally polarized pattern for WLAN applications," in *Proc. 33rd Eur. Microwave Conf.*, Munich, 2003, pp. 1275–1278.

[14] C. C. Lin, L. C. Kuo, and H. R. Chuang, "A horizontally polarized omnidirectional printed antenna for WLAN applications," *IEEE Trans. Antennas Propag.*, vol. 54, no. 11, pt. 2, pp. 3551–3556, Nov. 2006.

[15] C. H. Ahn, S. W. Oh, and K. Chang, "A dual-frequency omnidirectional antenna for polarization diversity of MIMO and wireless communication applications," *IEEE Antennas Wireless Propag. Lett.*, vol. 8, pp. 966–970, 2009.

[16] C. Caloz and T. Itoh, "Transmission line approach of left-handed (LH) materials and microstrip implementation of an artificial LH transmission line," *IEEE Trans. Antennas Propag.*, vol. 52, no. 5, pp. 1159–1166, May 2007.
[17] G. V. Eleftheriades and K. G. Balmain, *Negative-Refraction Metamaterials: Fundamental Principles and Applications*. Hoboken, NJ: Wiley-IEEE Press, 2005.
[18] C. Caloz and T. Itoh, *Electromagnetic Metamaterials: Transmission Line Theory and Microwave Applications*. Hoboken, NJ: Wiley-IEEE Press, 2005.
[19] A. Sanada, C. Caloz, and T. Itoh, "Zeroth order resonance in composite right/left-handed transmission line resonators," in *Proc. Asia-Pacific Microwave Conf.*, Seoul, Korea, Nov. 2003, vol. 3, pp. 1588–1592.
[20] A. L. Borjia, P. S. Hall, and Q. Liu, "Omnidirectional loop antenna with left-handed loading," *IEEE Antennas Wireless Propag. Lett.*, vol. 6, pp. 495–498, 2007.
[21] D. M. Dobkin, S. M. Weigand, and N. Iyec, "Segmented magnetic antennas for near-field UHF RFID," *Microw. J.*, vol. 50, no. 6, Jun. 2007.
[22] X. Li, J. Liao, Y. Yuan, and D. Yu, "Segmented coupling eye-shape UHF band near field antenna design," in *Proc. Asia-Pacific Microwave Conf.*, Singapore, Dec. 2009, pp. 2401–2404.
[23] X. Qing, C. K. Goh, and Z. N. Chen, "Segmented loop antenna for UHF near-field RFID applications," *Electron. Lett.*, vol. 45, no. 17, Aug. 2009.
[24] X. Qing, Z. N. Chen, and C. K. Goh, "UHF near-field RFID reader antenna with capacitive couplers," *Electron. Lett.*, vol. 46, no. 24, Nov. 2010.
[25] X. Qing, C. K. Goh, and Z. N. Chen, "A broadband UHF near-field RFID antenna," *IEEE Trans. Antennas Propag.*, vol. 58, no. 12, pp. 3829–3838, Dec. 2010.
[26] D. M. Pozar, *Microwave Engineering*, 3rd ed. Hoboken, NJ: Wiley, 2005.

Kunpeng Wei, photograph and biography not available at the time of publication.

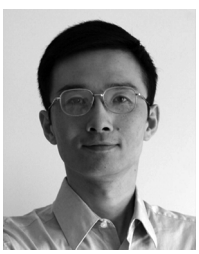

Zhijun Zhang (M'00–SM'04) received the B.S. and M.S. degrees from the University of Electronic Science and Technology of China (UESTC), Chengdu, in 1992 and 1995, respectively, and the Ph.D. degree from Tsinghua University, Beijing, China, in 1999.

In 1999, he was a Postdoctoral Fellow with the Department of Electrical Engineering, University of Utah, Salt Lake City, where he was appointed a Research Assistant Professor in 2001. In May 2002, he was an Assistant Researcher with the University of Hawaii at Manoa, Honolulu. In November 2002, he joined Amphenol T&M Antennas, Vernon Hills, IL, as a Senior Staff Antenna Development Engineer and was then promoted to the position of Antenna Engineer Manager. In 2004, he joined Nokia Inc., San Diego, CA, as a Senior Antenna Design Engineer. In 2006, he joined Apple Inc., Cupertino, CA, as a Senior Antenna Design Engineer and was then promoted to the position of Principal Antenna Engineer. Since August 2007, he has been with the Department of Electronic Engineering, Tsinghua University, Beijing, China, where he is a Professor.

Zhenghe Feng (SM'92–F'12) received the B.S. degree in radio and electronics from Tsinghua University, Beijing, China, in 1970.

Since 1970, he has been with Tsinghua University, as an Assistant, Lecturer, Associate Professor, and Full Professor. His main research areas include numerical techniques and computational electromagnetics, RF and microwave circuits and antenna, wireless communications, smart antenna, and spatial temporal signal processing.

Magdy F. Iskander (F'91–LF'12) is the Director of the Hawaii Center for Advanced Communications (HCAC), College of Engineering, University of Hawaii at Manoa, Honolulu, Hawaii http://hcac.hawaii.edu. He is also a Co-director of the NSF Industry/University joint Cooperative Research Center between the University of Hawaii and four other universities in the US. From 1997–99 he was a Program Director at the National Science Foundation, where he formulated and directed a "Wireless Information Technology" Initiative in the Engineering Directorate. He spent sabbaticals and other short leaves at Polytechnic University of New York; Ecole Superieure D'Electricite, France; UCLA; Harvey Mudd College; Tokyo Institute of Technology; Polytechnic University of Catalunya, Spain; University of Nice-Sophia Antipolis, and Tsinghua University, China. He authored a textbook *Electromagnetic Fields and Waves* (Prentice Hall, 1992; and Waveland Press, 2001); edited the *CAEME Software Books*, Vol. I, 1991, and Vol. II, 1994; and edited four other books on *Microwave Processing of Materials*, all published by the Materials Research Society, 1990–1996. He has published over 200 papers in technical journals, holds eight patents, and has made numerous presentations in International conferences. He is the founding editor of the journal *Computer Applications in Engineering Education* (CAE). His research focus is on antenna design and propagation modeling for wireless communications and radar systems, and in computational electromagnetic.

Dr. Iskander is a Life Fellow of the IEEE. He was the 2002 President of the IEEE Antennas and Propagation Society, and was a member of the IEEE APS AdCom from 1997 to 1999, and 2003–2006. He was the General Chair of the 2000 IEEE AP-S Symposium and URSI Meeting, and the 2003, 2005, 2007, and 2010 IEEE Wireless Communications Technology Conferences in Hawaii. He was also a Distinguished Lecturer for the IEEE AP-S (1994–97) and during this period he gave lectures in Brazil, France, Spain, China, Japan, and at a large number of US universities and IEEE chapters. He is a IEEE Fellow 1991. He received the 2010 University Of Hawaii Board Of Regents' Medal for Excellence in Teaching and the University of Utah Distinguished Teaching Award in 2000. He also received the 1985 Curtis W. McGraw ASEE National Research Award, 1991 ASEE George Westinghouse National Education Award, 1992 Richard R. Stoddard Award from the IEEE EMC Society. He was a member of the 1999 WTEC panel on "Wireless Information Technology-Europe and Japan," and chaired two International Technology Institute panels on "Asian Telecommunication Technology" sponsored by DoD in 2001 and 2003. He co-edited two special issues of the IEEE TRANSACTIONS ON ANTENNAS AND PROPAGATION on Wireless Communications Technology, 2002 and 2006, and co-edited a special issue of the *IEICE Journal* in Japan in 2004.